Rheol Acta (2010) 49:237–243
DOI 10.1007/s00397-009-0394-4

ORIGINAL CONTRIBUTION

Poiseuille flow and drop circulation in microchannels

Steven D. Hudson

Received: 19 July 2009 / Accepted: 5 October 2009 / Published online: 21 October 2009

Abstract Microfluidics aims to control precisely the transport of fluids and suspended particles or drops. Two characteristics of such transport in rectangular microchannels are addressed here, as a function of the cross-sectional aspect ratio. First, we highlight a convenient expression for the ratio of the centerline to bulk flow velocities, which is relevant for controlling the flow of suspended or flow-focused objects. Then, using the theory of Nadim and Stone, the droplet circulation fountain-flow pattern in such channels is evaluated explicitly, and implications for interfacial mobility measurements are discussed. For example, when the interface is retarded, part of the fountain reverses direction, thus alleviating stagnation, promoting mixing, and reducing interfacial concentration gradients.

Keywords Microfluidics · Multiphase flow · Droplets · Interfacial retardation · Marangoni flow

Introduction

The rise of microfluidic applications drives a need to determine flow parameters for cross-sectional geometries produced by various fabrication procedures (Mortensen et al. 2005). For devices made by soft lithography, rectangular channels are the most common, and rectangular ducts are common in other microsystems also. In rectangular channels, the ratio of channel width w and height h controls flow parameters such as the hydraulic resistance and flow profile. Here, we discuss these parameters and instructive approximations.

The cross-sectional geometry also influences the behavior of drops, which often are used in microfluidics (Teh et al. 2008). Microfluidics are excellent for controlling the production of drops (Thorsen et al. 2001; Anna et al. 2003) and, in turn, the production of particles (Xu et al. 2005; Nie et al. 2006), aggregates, or vesicles (Shum et al. 2008), and for the measurement of droplet and interfacial properties (Cabral and Hudson 2006; Hudson et al. 2005; Martin and Hudson 2009). Drops are also used to control mass transfer: either to confine and mix (Song et al. 2003) or exchange (Mary et al. 2008) molecular components. Some applications (e.g., biological (He et al. 2005)) contain complex mixtures involving many components, which transfer within, to, and across phase boundaries.

In many of these applications, the drop circulation rate and flow type are significant to mixing and mass transfer. Moreover, heat transfer in two-phase flow and the drag coefficient (or slip velocity) of droplets are affected by drop circulation. Interfacial mobility and mass transfer also influence drop formation and associated processes such as tip streaming (Anna et al. 2003; Anna and Mayer 2006; Lee et al. 2009).

Consequently, the flow of drops is of interest. The flow inside and outside nearly spherical drops has been determined in linear and nonlinear flow fields: Taylor calculated it for simple shear and extensional flow (Taylor 1932, 1934), and Hetsroni et al. calculated it for nonlinear flow (Hetsroni and Haber 1970). It is expressed in simplest terms by Nadim and Stone (1991),

S. D. Hudson (✉)
Complex Fluids Group, Polymers Division,
National Institute of Standards and Technology,
100 Bureau Dr., Gaithersburg, MD 20899-8542, USA
e-mail: steven.hudson@nist.gov

and this calculation is used here to determine drop circulation produced by Poiseuille flow in rectangular channels. Our result serves as a reference point for comparison, when drop circulation and interfacial rheology is complicated by surfactant effects.

In this brief paper, the effect of channel aspect ratio w/h is explored, and analysis proceeds from single-phase velocity profiles to drop circulation and flow behavior. The former motivates the velocity scaling used for the latter.

Review of geometrical effect on the ratio of centerline and average velocities

An important quantity describing a microchannel is its hydraulic resistance R_h, which determines the volumetric flow rate Q through the channel and is, therefore, naturally related to the average flow velocity u_{avg} in the channel.

$$R_h = \frac{\Delta p}{Q};\ u_{avg} = \frac{Q}{A};\ R_h^* = \frac{\eta L}{A^2};\ R_h = \alpha R_h^*, \tag{1}$$

where η is the fluid viscosity, A is the cross-sectional area of the channel, and Δp is the pressure drop along the channel length L. In general, to compute this resistance, we must integrate the flow field in the channel.

For a straight channel, the Navier–Stokes equation reduces to the Poisson equation, which in a rectangular geometry (channel width w and height h) has the following solution (Berker 1963):

$$\mathbf{u} = \mathbf{k}\frac{\Delta p}{\eta L}\frac{4h^2}{\pi^3}\sum_{n=1,3,5,\ldots}^{\infty}(-1)^{(n-1)/2} \times \frac{1}{n^3}\left(1-\frac{\cosh\left(n\pi x/h\right)}{\cosh\left(n\pi w/2h\right)}\right)\cos\left(n\pi y/h\right) \tag{2}$$

In this geometry, the maximum velocity u_{max} is on the central axis (here defined as $x = y = 0$); $\mathbf{k}$ is the unit vector along the channel. Integrating the velocity field over the channel cross section, the average velocity u_{avg} and hydraulic resistance of the channel may be determined.

When the fluid contains an object of interest (such as a particle, droplet, or molecule) on the centerline, it is useful to know both the average and maximum flow rates in the channel (in the case of a droplet, its velocity is very nearly the maximum velocity, when either the relative viscosity or the size of the drop are small (Hetsroni et al. 1970). That is, its slip velocity is very small). Using Eqs. 1 and 2 and identities for sums of reciprocal powers (Abramowitz and Stegun 1972), the ratio of the two characteristic velocities can be determined.

$$\frac{u_{max}}{u_{avg}} = \frac{3}{2}\left(1-\frac{32}{\pi^3}\sum_{n=1,3,5,\ldots}^{\infty}(-1)^{(n-1)/2}\frac{1}{n^3}\frac{1}{\cosh\left(n\pi w/2h\right)}\right) \times\left(1-\frac{192}{\pi^5}\frac{h}{w}\sum_{n=1,3,5,\ldots}^{\infty}\frac{1}{n^5}\tanh\left(n\pi w/2h\right)\right)^{-1} \tag{3}$$

For flow between infinite parallel plates, $w >> h$, this ratio is known to be 1.5. Equation 3 demonstrates, however, that this limit is approached very slowly (Fig. 1). The difference from the limit is not a substantial one in terms of the flow profile (Fig. 1, inset); instead, the difference merely manifests an effectively reduced area due to the edges of a slit channel (Chatwin and Sullivan 1982). The velocity profile in the central region matches the infinite slit flow profile very closely (Fig. 1, inset; the disagreement is less than 1% when $w/h > 3.4$), and a reduced flow rate is focused at the channel edges. Thus, the ratio u_{max}/u_{avg} and other quantities of Eq. 1 for modest w/h are predicted well by a reduction in the effective area (Berker 1963; Chatwin and Sullivan 1982), so that

$$\frac{u_{max}}{u_{avg}} = \frac{3}{2}\frac{w}{w_{eff}};\ \alpha = \frac{12w^2}{w_{eff}h};\ R_h = \frac{12\eta L}{w_{eff}h^3} \tag{4}$$

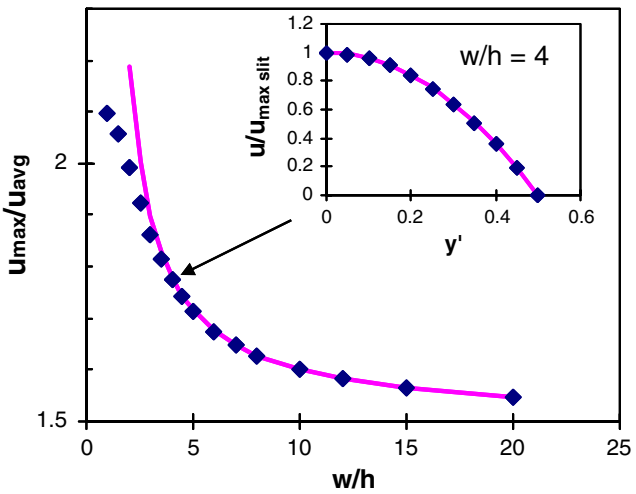

Fig. 1 The relationship between the volumetric and centerline flow rates in rectangular channels (*symbols*, Eq. 3). *Inset* is the velocity profile along $x = 0$ for $w/h = 4$ (*symbols*, Eq. 2), which matches the slit flow limit ($w/h >> 1$, *curve*) to much better than 1%. For this channel geometry, $u_{max}/u_{avg} = 1.8$ is much larger than the slit flow limit ratio, equal to 1.5. This difference is easily accounted for by a correction to the effective area (the *curve*, Eqs. 4 and 5)

where the effective reduction in width, $w - w_{\text{eff}}$, is calculated from Eq. 3, in the limit $w/h >> 1$, resulting in the following expression, involving the Riemann zeta function ζ:

$$w - w_{\text{eff}} = h\frac{192}{\pi^5}\sum_{n=1,3,5,\ldots}^{\infty}\frac{1}{n^5} = h\frac{186}{\pi^5}\zeta\,(5) \cong h\cdot 0.630\ldots. \tag{5}$$

A close approximation of $w - w_{\text{eff}}$ (0.1% difference) is also obtained by integrating Eq. 2 along x (for $y = 0$ and $w/h >> 1$). Thus, the volumetric flow in a channel of width w and height h is equivalent to that in an infinite slit through a section of width w_{eff} (as indicated by the line in Fig. 1).

Finally, since $u_{\max}$ approaches the slit limit much more rapidly than u_{avg}, the former is the preferred choice for scaling the velocity in the subsequent section.

Geometrical effect on drop circulation

A drop near the centerline in Poiseuille flow experiences an internal fountain-flow circulation in which its fluid flows forward through the center and back along the surface to the rear (Fig. 2). This recirculation is of interest in terms of heat and mass transfer (Alves et al. 2005). This recirculation is also an indication of interfacial rheology and Marangoni effects.

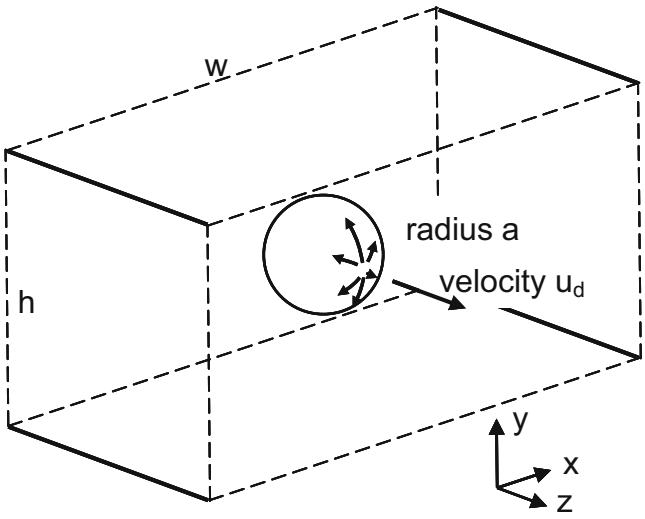

Fig. 2 Schematic of the Poiseuille flow geometry: a drop of radius a on the centerline of a channel of width w and height h, with a pressure gradient along z, the channel direction. The translational velocity of the drop is u_d. The fluid in the drop circulates in a fountain-flow pattern, so that convection relative to the drop center is towards the nose, there diverges along the interface, then converges towards the rear and returns to the center

The starting point for calculating the flow field in the drop is the undisturbed flow (Eq. 2), which we rewrite in dimensionless form:

$$\tilde{\mathbf{u}} = \frac{\mathbf{u}}{u_{\max}} = \mathbf{k}\frac{\sum_{n=1,3,5,\ldots}^{\infty}(-1)^{(n-1)/2}\frac{1}{n^3}\left(1-\frac{\cosh\left(n\pi x/h\right)}{\cosh\left(n\pi w/2h\right)}\right)\cos\left(n\pi y/h\right)}{\sum_{n=1,3,5,\ldots}^{\infty}(-1)^{(n-1)/2}\frac{1}{n^3}\left(1-\frac{1}{\cosh\left(n\pi w/2h\right)}\right)} \tag{6}$$

In the following expressions, length is made dimensionless by the drop radius a and velocity by $u_{\max}$. One useful dimensionless parameter here is what we will call the confinement parameter ($2a/h$), the ratio of the drop diameter to the minimum dimension of the channel cross section. Using the expressions derived by Nadim and Stone (1991), valid for small values of this ratio, we calculate the flow field in the drop. For large values of confinement (approaching and exceeding unity), flow and deformation of drops have been explored using boundary integral calculations (Griggs et al. 2007).

The undisturbed flow field may be expressed in a Taylor expansion to second order:

$$\tilde{\mathbf{u}}\,(\mathbf{r}) = \mathbf{U} + \boldsymbol{\Omega}\times\mathbf{r} + \mathbf{r}\cdot\mathbf{E} + \mathbf{rr}:\mathbf{K} + \ldots, \tag{7}$$

where linear flows are described by the first three terms. In Poiseuille flow, the last term is important. The linear terms are zero for drops on the centerline and finite for those off of that line. In either instance, $\mathbf{K}$ is given by:

$$\mathbf{K} = \frac{1}{2}a^2\nabla\nabla\tilde{\mathbf{u}}, \tag{8}$$

which can be evaluated from Eq. 6 and expressed in terms of three components, of first, second, and third rank (Nadim and Stone 1991):

$$\begin{aligned}\tau_l &= K_{ppl},\\ \theta_{lm} &= K_{lpq}\varepsilon_{qpm} + K_{mpq}\varepsilon_{qpl},\\ \gamma_{ijk} &= \left(K_{ijk} + K_{kij} + K_{jki}\right)/3\\ &\quad -\left(\delta_{ij}K_{ppk} + \delta_{ik}K_{ppj} + \delta_{jk}K_{ppi}\right)/15.\end{aligned} \tag{9}$$

From these, the flow field in the drop $\mathbf{u}_{\text{circ}}$ (in the reference frame of the drop center of mass) can be calculated from the expressions of Nadim and Stone (1991).

$$\hat{\mathbf{u}}\cdot(1+\lambda)=\frac{\mathbf{u}_{\text{circ}}(1+\lambda)}{u_{\max}(2a/h)^2}=\left(-\frac{5}{2}+\frac{15}{4}r^2\right)\mathbf{rr}:\boldsymbol{\gamma}-\frac{5}{4}\mathbf{rrrr}(\cdot)^3\boldsymbol{\gamma}+\frac{5}{3}\left(\frac{1+\lambda}{4+\lambda}\right)\mathbf{r}\times(\mathbf{r}\cdot\boldsymbol{\theta})-\frac{1}{2}\mathbf{rr}\cdot\boldsymbol{\tau}+\left(-\frac{1}{2}+r^2\right)\boldsymbol{\tau} \tag{10}$$

For convenience, we have here and henceforth rescaled K by dividing by $(2a/h)^2$. The relative viscosity of the drop is λ. In general, nonzero components of K are K_{113}, $K_{123}=K_{213}$, and K_{223}. If the drop is off the centerline, the linear flow solution (Stone et al. 1991) is added. We will consider here drops on the centerline, where also $K_{123}=0$.

As noted above (Fig. 2), drop circulation $\hat{\mathbf{u}}$ is a fountain flow, and its dependence on w/h and λ is summarized here. In the center of the drop, flow is towards the leading nose of the drop. From Eq. 10, this flow $\hat{\mathbf{u}}_o$ is

$$\hat{\mathbf{u}}_o=-\frac{1}{2}\boldsymbol{\tau}/(1+\lambda)=-\mathbf{k}\frac{1}{2}(K_{113}+K_{223})/(1+\lambda) \tag{11}$$

The magnitude of this flow depends on the aspect ratio of the channel. For wide channels, it is approximately 0.5, whereas for square channels, it is approximately 0.85, which is close to unity, as for a circular channel. Stagnation points occur at the poles of the drop, $\pm\,\mathbf{k}$, i.e., at its leading nose and its tail. Fluid returns to the rear of the drop around its periphery. At the equator, the flow is of course again along the z axis, net negative (towards the rear), and given by:

$$\hat{u}_{\text{equator}}=\left\{\frac{5}{8}(K_{113}+K_{223})+(K_{113}-K_{223})\cos(2\psi)\times\left[\frac{5}{24}+\frac{5}{3}\left(\frac{1+\lambda}{4+\lambda}\right)\right]\right\}\Big/(1+\lambda) \tag{12}$$

where ψ is the azimuthal angle. Figure 3 plots $\hat{u}_{\text{equator}}$ vs. w/h for three values of ψ, i.e., 0, $\pi/4$ and $\pi/2$, denoted $\hat{u}_x$, $\hat{u}_{xy}$, and $\hat{u}_y$, respectively. $\hat{u}_{xy}$ is also the average equatorial velocity. Since the internal flow is dictated by the drop's interfacial motion, there is a fixed relationship between $\hat{u}_{xy}$ and $\hat{u}_0$, i.e.

$$\hat{u}_0=-\frac{4}{5}\hat{u}_{xy}. \tag{13}$$

From Eqs. 6 and 8, the coefficients $K_{113}+K_{223}$ and $K_{113}-K_{223}$ are calculated.

$$K_{113}+K_{223}=-\left(1-\frac{32}{\pi^3}\sum_{n=1,3,5,\ldots}^{\infty}(-1)^{(n-1)/2}\times\frac{1}{n^3}\frac{1}{\cosh(n\pi w/2h)}\right)^{-1}$$

$$K_{113}-K_{223}=-(K_{113}+K_{223})\left(1-\frac{8}{\pi}\sum_{n=1,3,5,\ldots}^{\infty}(-1)^{(n-1)/2}\times\frac{1}{n}\frac{1}{\cosh(n\pi w/2h)}\right) \tag{14}$$

For slit flow $K_{113}=0$ and $K_{223}=-1$. When the channel is square, $K_{113}=K_{223}\cong-0.85$, and the drop circulation is similar to that in a circular channel. Furthermore,

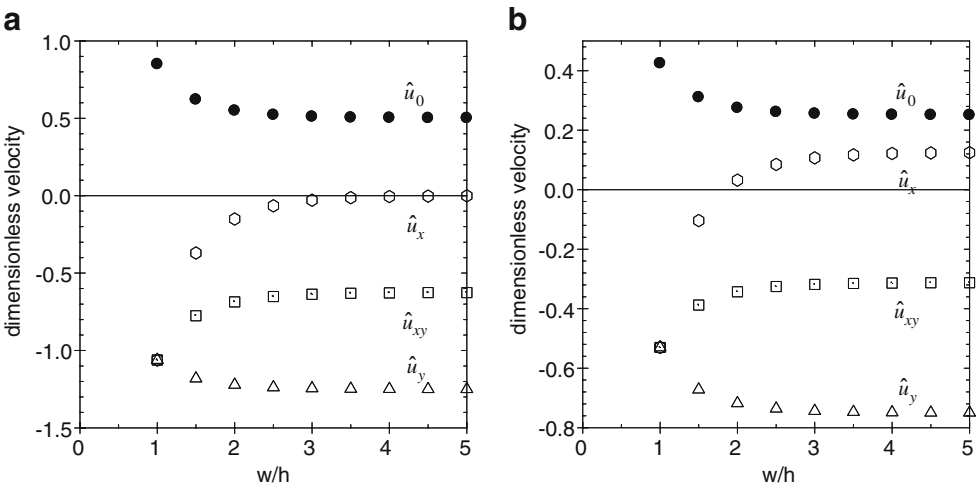

Fig. 3 Dimensionless drop circulation velocities as a function of channel cross section aspect ratio w/h, at the drop center $\hat{\mathbf{u}}_o=\hat{\mathbf{u}}(\mathbf{r}=\mathbf{0})$ (*filled circles*) and equator, viz. at the side $\hat{\mathbf{u}}_x=\hat{\mathbf{u}}(\mathbf{r}=a\mathbf{i})$ (*hexagons*), *top* $\hat{\mathbf{u}}_y=\hat{\mathbf{u}}(a\mathbf{j})$ (*triangles*), and intermediate $\hat{\mathbf{u}}_{xy}=\hat{\mathbf{u}}\left((\mathbf{i}+\mathbf{j})\,a/\sqrt{2}\right)$ locations; see text and Eq. 12. Viscosity ratio equal to 0 and 1 are depicted in **a** and **b** respectively

when comparing square and circular channels of the same hydraulic resistance, the respective magnitudes of the drop circulation velocity differ only by approximately 1.6%.

When the viscosity ratio is zero, the equatorial velocity $\hat{u}_x$ approaches zero in the slit channel limit (Fig. 3). When the viscosity ratio is finite, however, this velocity is greater than zero, i.e., towards the leading nose of the drop. This velocity can even exceed that at the drop center when $\lambda > 8/3$ (Eqs. 12 and 13). Although these calculations are for a drop on the centerline, we note that this is not a stable location of the drop when the viscosity ratio is between 0.5 and 10 (Chan and Leal 1979; Hiller and Kowalewski 1987). In these cases, the drop migrates slowly from the centerline. When the drop does migrate off the center, a complete calculation would include the linear flow terms.

Discussion

Measurement considerations for characterization of drop circulation

What measurements are necessary to characterize the circulation in the drop? Based on Eqs. 12 and 13, a measurement of $\hat{\mathbf{u}}_o$ and either $\hat{\mathbf{u}}_x$ or $\hat{\mathbf{u}}_y$, for example, is sufficient for complete characterization.

Since the drop is stress-free, its translational velocity u_d is also related to the circulation velocities.

$$u_d/u_{\max} = 1 + \tau \left(\frac{2a}{h}\right)^2 \frac{\lambda}{(2+3\lambda)} \tag{15}$$

In particular, the relative slip velocity (the second term) and the average equatorial velocity are both proportional to $\tau = K_{113} + K_{223}$. Thus, one measure of the drop circulation is accessible from the drop speed, even without particle tracers within the drop. This approach is impractical, however, since the relative slip velocity is small when the drop radius a, or relative viscosity λ are small. Particle image velocimetry relative to the drop center of mass then is a more viable approach, as well as yielding more information about the flow field in the drop, which will either confirm these calculations or indicate other effects of confinement or Marangoni forces as noted below.

Mixing in drop

Since the circulation pattern depends qualitatively on the channel aspect ratio, mixing in drops can be enhanced in a channel where its aspect ratio and orientation vary along its length, so that blinking vortices can be induced.

Symmetry breaking

When the channel is square, the velocity of the interface is the same everywhere on the drop equator (Eq. 12), just as it is in a circular tube. Numerical calculations (not reported) indicate that this symmetry is broken by confinement, and a higher-order cosine perturbation of Eq. 12 arises. When $2a/h = 0.4$, the $\cos 4\psi$ term has an amplitude that is merely a few percent of the average equatorial velocity. Perhaps this mode may be enhanced when Marangoni forces are active. This mode may or may not also change the ratios between the average equatorial velocity and either the slip velocity or $\hat{\mathbf{u}}_o$.

Marangoni effects

As just noted, Marangoni forces can perturb the drop circulation. Principally, their effect is analogous to the droplet viscosity (Milliken et al. 1993), because internal flow and interfacial motion are directly coupled. When Marangoni forces resist the applied force, their effect is like an increase in drop viscosity and in proportion to the so-called interfacial retardation A, which is equal to the product of the Marangoni number and the effective interfacial Peclet number (Ramirez and Davis 1999; Blawzdziewicz et al. 1999; Hudson et al. 2003).

As the circulation pattern in the drop depends on viscosity ratio, similar effects are thus anticipated with Marangoni-induced interfacial retardation. These include, in particular, the qualitative changes in flow at $\pm\mathbf{i}$ (Fig. 3). For wide channels and low viscosity ratio, the flow there is nearly zero. For isometric cross section, the flow is towards the back. However, for wide channels and more viscous drops, the flow there is towards the nose. These qualitative changes are likely to be a sensitive measure of the interfacial retardation. They also bear on mixing (both interfacial and internal), interfacial concentration gradients, and droplet slip velocity.

Although the interfacial-bulk analogy holds to some point, eventually the analogy breaks down. In the case of interfacial retardation, the interior remains fluid and perhaps additional modes of circulation can occur, e.g., an increase in higher order cosine perturbations, as suggested above. In the limit of inviscid drops with incompressible interfaces, divergence on the interface will be zero; yet, the flow may still be substantial. Recent experiments in our lab confirm this

conjecture: in that case, the flow $\hat{u}_x$ was remarkably large 0.41 ± 0.05, even when $\hat{u}_0$ was essentially zero. In addition, the proportionality to Marangoni and Peclet numbers breaks down at high surfactant concentration, when the interface becomes remobilized (Stebe et al. 1991; Stebe and Maldarelli 1994).

Flow focusing

As channel geometry dictates different circulation patterns in free drops, similar effects will occur when bound to an orifice, as in flow focusing and thus will influence drop formation and tip-streaming phenomena (Anna and Mayer 2006). Circular (Utada et al. 2005; Ganan-Calvo and Gordillo 2001) and thin rectangular (Anna et al. 2003; Lee et al. 2009) flow-focusing geometries have been employed. By implication of the calculations reported here in this report, these differences in channel and orifice geometry affect the circulation in the drop fluid before detachment. As a consequence, therefore, of inducing different infacial tension gradients, the drop size, the transition between steady and unsteady regimes (Cheng et al. 2006), and the characteristics (e.g., period) of the unsteady regimes (Anna and Mayer 2006) will be affected likewise by geometry.

Conclusions

The circulation patterns of drops flowing in rectangular microchannels are evaluated explicitly here. Notably, when the interface is retarded by droplet viscosity, part of the fountain reverses direction. This calculation serves as a reference point for comparison of instances when the interface is retarded, whether by surfactant compressibility or viscosity. Such comparisons are expected to demonstrate qualitative and quantitative differences.

References

Abramowitz M, Stegun IA (eds) (1972) Handbook of mathematical functions with formulas, graphs, and mathematical tables US Govt. Print. Off., Washington

Alves SS, Orvalho SP, Vasconcelos JMT (2005) Effect of bubble contamination on rise velocity and mass transfer. Chem Eng Sci 60:1–9

Anna SL, Bontoux N, Stone HA (2003) Formation of dispersions using "flow focusing" in microchannels. Appl Phys Lett 82:364–366

Anna SL, Mayer HC (2006) Microscale tipstreaming in a microfluidic flow focusing device. Phys Fluids 18:121512

Berker R (1963) Integration des equations du mouvement d'un fluide visqueux incompressible. In: Flugge S, Truesdell CA (eds) Handbuch der physik, vol 8, part 2, fluid dynamics. Springer, Berlin, pp 1–384

Blawzdziewicz J, Wajnryb E, Loewenberg M (1999) Hydrodynamic interactions and collision efficiencies of spherical drops covered with an incompressible surfactant film. J Fluid Mech 395:29–59

Cabral JT, Hudson SD (2006) Microfluidic approach for rapid multicomponent interfacial tensiometry. Lab Chip 6:427–436

Chan PCH, Leal LG (1979) Motion of a deformable drop in a 2nd-order fluid. J Fluid Mech 92:131–170

Chatwin PC, Sullivan PJ (1982) The effect of aspect ratio on longitudinal diffusivity in rectangular channels. J Fluid Mech 120:347–358

Cheng ZD, Cristal G, Link DR, Brenner M, Stone HD, Weitz DA (2006) Dynamics of drop production in hydrodynamic flow focusing microfluidic devices: periodic behaviors and chaos. In: Proceeding of the 4th International conference on computing, communications and control technologies, Orlando, FL

Ganan-Calvo AM, Gordillo JM (2001) Perfectly monodisperse microbubbling by capillary flow focusing. Phys Rev Lett 87:274501

Griggs AJ, Zinchenko AZ, Davis RH (2007) Low-Reynolds-number motion of a deformable drop between two parallel plane walls. Int J Multiph Flow 33:182–206

He MY, Edgar JS, Jeffries GDM, Lorenz RM, Shelby JP, Chiu DT (2005) Selective encapsulation of single cells and subcellular organelles into picoliter- and femtoliter-volume droplets. Anal Chem 77:1539–1544

Hetsroni G, Haber S (1970) The flow in and around a droplet or bubble submerged in an unbound arbitrary velocity field. Rheol Acta 9:488–496

Hetsroni G, Haber S, Wacholder E (1970) The flow field in and around a droplet moving axially within a tube. J Fluid Mech 41:689

Hiller W, Kowalewski TA (1987) An experimental study of the lateral migration of a droplet in a creeping flow. Exp Fluids 5:43–48

Hudson SD, Cabral JT, Goodrum Jr WJ, Beers KL, Amis EJ (2005) Microfluidic interfacial tensiometry. Appl Phys Lett 87:081905

Hudson SD, Jamieson AM, Burkhart BE (2003) The effect of surfactant on the efficiency of shear-induced drop coalescence. J Colloid Interface Sci 265:409–421

Lee W, Walker LM, Anna SL (2009) Role of geometry and fluid properties in droplet and thread formation processes in planar flow focusing. Phys Fluids 21:032103

Martin JD, Hudson SD (2009) Mass transfer and interfacial properties in two-phase microchannel flows. New J Phys 11 (in press)

Mary P, Studer V, Tabeling P (2008) Microfluidic droplet-based liquid-liquid extraction. Anal Chem 80:2680–2687

Milliken WJ, Stone HA, Leal LG (1993) The effect of surfactant on the transient motion of newtonian drops. Phys Fluids, A Fluid Dyn 5:69–79

Mortensen NA, Okkels F, Bruus H (2005) Reexamination of Hagen-Poiseuille flow: shape dependence of the hydraulic resistance in microchannels. Physical Review E 71:057301

Nadim A, Stone HA (1991) The motion of small particles and droplets in quadratic flows. Stud Appl Math 85:53–73

Nie ZH, Li W, Seo M, Xu SQ, Kumacheva E (2006) Janus and ternary particles generated by microfluidic synthesis: design, synthesis, and self-assembly. J Am Chem Soc 128:9408–9412

Ramirez JA, Davis RH (1999) Mass transfer to a surfactant-covered bubble or drop. AIChE J 45:1355–1358

Shum HC, Lee D, Yoon I, Kodger T, Weitz DA (2008) Double emulsion templated monodisperse phospholipid vesicles. Langmuir 24:7651–7653

Song H, Tice JD, Ismagilov RF (2003) A microfluidic system for controlling reaction networks in time. Angew Chem - International Edition 42:768–772

Stebe KJ, Maldarelli C (1994) Remobilizing surfactant retarded fluid particle interfaces.2. Controlling the surface mobility at interfaces of solutions containing surface-active components. J Colloid Interface Sci 163:177–189

Stebe KJ, Lin SY, Maldarelli C (1991) Remobilizing surfactant retarded fluid particle interfaces .1. Stress-free conditions at the interfaces of micellar solutions of surfactants with fast sorption kinetics. Phys Fluids, A Fluid Dyn 3:3–20

Stone HA, Nadim A, Strogatz SH (1991) Chaotic streamlines inside drops immersed in steady stokes flows. J Fluid Mech 232:629–646

Taylor GI (1932) The viscosity of a fluid containing small drops of another fluid. Proc R Soc Lond A 138:41–48

Taylor GI (1934) The formation of emulsion in definable fields of flow. Proc R Soc Lond A 146:501–523

Teh SY, Lin R, Hung LH, Lee AP (2008) Droplet microfluidics. Lab Chip 8:198–220

Thorsen T, Roberts RW, Arnold FH, Quake SR (2001) Dynamic pattern formation in a vesicle-generating microfluidic device. Phys Rev Lett 86:4163–4166.

Utada AS, Lorenceau E, Link DR, Kaplan PD, Stone HA, Weitz DA (2005) Monodisperse double emulsions generated from a microcapillary device. Science 308:537–541

Xu SQ, Nie ZH, Seo M, Lewis P, Kumacheva E, Stone HA, Garstecki P, Weibel DB, Gitlin I et al (2005) Generation of monodisperse particles by using microfluidics: control over size, shape, and composition. Angew Chem - International Edition 44:724–728